Revision 2

Microtexture investigation of amblygonite–montebrasite series with lacroixite: Characteristics and formation process in pegmatites

Yohei Shirose *,[1] and Seiichiro Uehara

Department of Earth and Planetary Sciences, Faculty of Sciences, Kyushu University, Fukuoka 819-0395, Japan

* E-mail: shirose.yohei.6n@kyoto-u.ac.jp

Abstract

Amblygonite–montebrasite series and lacroixite from Nagatare Li–Cs–Ta (LCT) pegmatite, Fukuoka Prefecture, Japan, were investigated by powder X-ray diffraction (XRD), electron

[1] Present address: The Kyoto University Museum, Kyoto University, Kyoto 606-8501, Japan

microprobe analyses, and transmission electron microscope (TEM)/scanning transmission electron microscope (STEM) analyses. Scattered patchy or lamellar lacroixite was contained in montebrasite and amblygonite in all observed specimens. TEM/STEM observations revealed that the patchy and lamellar texture comprised lacroixite and low fluorine montebrasite having same crystal orientations as that of host montebrasite and the boundaries corresponded to well-developed {110} planes. The observed microtexture was newly discovered, and it is an important evidence of the exsolution process. In XRD experiments conducted at high temperature, the unit cell parameters of amblygonite were closer to that of monoclinic structures such as lacroixite with increasing temperature. Results suggested that scattered patches or lamellae of lacroixite were exsolution textures from a high-temperature phase.

Montebrasite and amblygonite specimens from other localities involved varying textures corresponding to their occurrence. The amblygonite–montebrasite series from petalite-bearing pegmatite included low to high lacroixite contents and that from lower-temperature pegmatite with spodumene either did not possess or involved low lacroixite contents. Gem-quality montebrasite from drusy vugs formed at low temperature did not include any exsolution texture or lacroixite. The variety of texture of the

amblygonite–montebrasite series indicated in this study generated new possibilities as the indicator of pegmatite-forming process.

Keywords: Amblygonite–montebrasite series; lacroixite; exsolution; Nagatare pegmatite; TEM

Introduction

The amblygonite–montebrasite series is widely considered to be primary phosphates occurring in Li–Cs–Ta enriched (LCT) (Černý and Ercit 2005) pegmatites and topaz-bearing granites (e.g., Černá et al. 1973; London et al. 2001). The chemical compositions correspond to a solid solution of $LiAl(PO_4)F$ (amblygonite) and $LiAl(PO_4)(OH)$ (montebrasite) with triclinic symmetry ($C\bar{1}$). Extant studies investigated the changes in mineralogical properties corresponding to the F/(F+OH) ratio and also indirectly examined quantitative determinations of the F/(F+OH) ratio with respect to mineralogical properties such as optical properties, XRD patterns, unit cell parameters, and Raman spectra (e.g., Černá et al. 1973; Kallio 1978; Greiner and Bloss 1987; Groat et al. 1990, 2003; Rondeau et al. 2006). Despite a complete solid solution, previous studies have

not documented the amblygonite end member. Moreover, the amblygonite–montebrasite series from pegmatites generally contain intermediate amounts of fluorine. This is restricted by the fluorine contents of pegmatite-forming melts based on the partitioning of fluorine between the amblygonite–montebrasite series and melt (London et al. 2001). Hydrothermal alteration of the primary amblygonite–montebrasite series to various secondary phosphates during the late stages of pegmatite formation was reported in a few pegmatites (London and Burt 1982; Baldwin et al. 2000; Galliski et al. 2012; Shirose and Uehara 2014). In these situations, secondary montebrasite is also produced along the fractures and cleavages in the primary amblygonite–montebrasite series. Secondary montebrasite indicates lower fluorine contents and higher interference color under a polarized microscope when compared with the corresponding properties of the primary amblygonite–montebrasite series (London and Burt 1982; Shirose and Uehara 2014). Typically, the amblygonite–montebrasite series has fine textures with lacroixite, $NaAl(PO_4)F$ with monoclinic symmetry ($C2/c$). Prior research discredited a species reported as "natromontebrasite," $(Na,Li)Al(PO_4)(OH,F)$ and indicated that it comprises a mixture of OH-rich amblygonite and lacroixite with subordinate amounts of wardite (Fransolet 1989; Fransolet et al. 2007). Groat et al. (1990) refined the crystal structure of the amblygonite–montebrasite series using a *C*-centered cell, and the

findings revealed that the pseudomonoclinic structure was topologically identical to the monoclinic structure of titanite group minerals including lacroixite. The study also pointed out that it was not possible to substitute the amblygonite–montebrasite series with sodium or calcium owing to crystal structure restrictions. In several cases, amblygonite–montebrasite crystals contain sodium components in the form of a fine lacroixite intergrowth. However, the formation process of the amblygonite–montebrasite series with patchy lacroixite is not clear. Although there are possibilities of exsolution, hydrothermal alteration textures, or simultaneous intergrowth, further detailed studies are required to understand crystallographic relationships between the amblygonite–montebrasite series and lacroixite. Thus, the present study examined the amblygonite–montebrasite series with lacroixite from an LCT pegmatite in Nagatare, Fukuoka Prefecture, Japan, using powder X-ray diffraction (XRD) experiments at room temperature and high temperatures, electron microprobe analyses (EPMA), and transmission electron microscope (TEM)/scanning transmission electron microscope (STEM) observations. The study described the crystallographic relationship between the amblygonite–montebrasite series and lacroixite and discussed the formation processes of their intergrowth textures. Furthermore, XRD and EPMA were used to investigate the amblygonite–montebrasite series from different

occurrences with specimens from other localities.

Geological background of Nagatare pegmatite

In the North part of the Kyushu region in Japan, Cretaceous granitoids are widely exposed and intrude into Sangun metamorphic rocks. The Nagatare pegmatite is a Li–Cs–Ta enriched (LCT) (Černý and Ercit 2005) pegmatite that is located at Nagatare in the western area of Fukuoka City, Fukuoka Prefecture. The pegmatite is derived from Sawara granite (100–80 Ma) that intrudes into the Itoshima granodiorite (115–70 Ma) (Karakida et al. 1994). Outcrops of barren and beryl-bearing pegmatites exist around a Li-enriched dyke from the Nagatare coast to Mt. Nagatare. These Li-mineral deficient pegmatites often occur with aplites. The pegmatites are 5–20 m in width with a dyke-shaped body and are concordant with the lamination structures of the Sawara granite. The Li-enriched pegmatite of Mt. Nagatare was mined for lithium in the middle of the 20th century. Some amount of the ores mined was stockpiled, although only a very small amount of remaining lithium ores currently exists. The body of the Li-enriched pegmatite was classified to several zones based on mineral paragenesis and inner texture. The Li-enriched pegmatite contains rare

element minerals such as "lepidolite" (polylithionite–trilithionite), Li-bearing tourmaline, petalite, montebrasite, amblygonite, and pollucite (e.g., Shibata 1934; Kuwano and Hikita 1967). Studies have reinvestigated the minerals of the Nagatare pegmatite including "lepidolite" (Kataoka and Uehara 2000), tourmaline (Shirose and Uehara 2013), the amblygonite–montebrasite series (Shirose and Uehara 2014), and other rare minerals such as bismuth minerals (Uehara and Shirose 2013). These rare minerals and lithium minerals occurred in the intermediate to core zone of the Li-enriched pegmatite.

Analytical methods

Eleven specimens of the amblygonite–montebrasite series used in the present study were collected from old ore deposits in the Nagatare pegmatite. These specimens correspond to the specimens used for a description of secondary phosphates (Shirose and Uehara 2014). Furthermore, specimens for comparison from other five pegmatite localities were analyzed. Eight specimens from five localities were used and included the Myokenzan pegmatite, Tanco pegmatite, Varuträsk pegmatite, Havey pegmatite, and Minas Gerais. Powder XRD data at room temperature were collected using a Bruker AXS M18XHF22-SRA

diffractometer that utilized monochromatized Cu*K*α radiation generated at 40 kV and 50 mA. The powders were prepared by grinding thin chips of the amblygonite–montebrasite series crystals within a few centimeters in length. Fluorine contents for the amblygonite–montebrasite series were estimated from bulk powder XRD patterns for all the specimens using Kallio's method (1978), and the average value of four equations used four reflections in the range of 46° and 56° 2θ Cu*K*α. The fluorine contents herein mean the bulk fluorine contents of the amblygonite–montebrasite series without the effects of other inclusion minerals. The powder XRD patterns simultaneously provided the lacroixite contents of amblygonite–montebrasite crystals based on a whole-powder-pattern fitting method using a Rigaku PDXL software. The amblygonite specimen from the Nagatare pegmatite with an internal chemical composition in the amblygonite–montebrasite series was heated from 50 °C to 700 °C, and the XRD patterns were measured in situ. The experiments were performed by a RIGAKU Ultima IV diffractometer with Cu*K*α radiation generated at 40 kV and 40 mA. The heating condition was set at 10 °C/min by a thermocouple under vacuum and was measured after holding at the target temperature for 10 min by the RIGAKU Ultima IV high temperature attachment. The unit cell parameters of the amblygonite specimen heated from 50 °C to 700 °C were calculated with Rietveld refinement in a

Rigaku PDXL software. Chemical analyses of polished thin sections were performed with a JEOL JXA8530F electron microprobe equipped with a wavelength dispersive X-ray spectrometer (WDS). Quantitative analyses were performed at an accelerating voltage of 15 kV, a beam current of 2 nA, and a probe diameter range of 5–15 μm. The standard materials corresponded to fluorphlogopite (for F*K*α), spodumene (for Al*K*α), $KTiOPO_4$ (for P*K*α), albite (for Na*K*α), diopside (Ca*K*α), and almandine (for Fe*K*α). The ZAF method was used for data correction. The Li_2O and H_2O contents were calculated from stoichiometry. The chemical composition of lacroixite involved analytical problems owing to its small diameter and beam damage. The EPMA observations of texture were also performed via backscattered electron (BSE) images, X-ray mapping images, and quantitative analyses with an energy dispersive X-ray spectrometer. Thin sections of montebrasite with lacroixite were ion-milled with Ar^+ ions using a GATAN Model 691 Precision Ion Polishing System such that they were electron transparent. TEM/STEM observations of the specimens were performed using a JEOL JEM-ARM200F operated at 200 kV. These instruments were located at the Ultramicroscopy Research Center in Kyushu University.

Results

Sample description and optical observation

Eleven specimens of the amblygonite–montebrasite series were collected from old ore deposits in the Nagatare pegmatite (Table 1). The sample numbers are listed with the analysis results in Table 1. Montebrasite and amblygonite from the Nagatare pegmatite typically occur as large subhedral to euhedral blocky crystals with lepidolite, Li-bearing tourmaline, and petalite included in quartz and albite (Fig. 1a; Table 1). Small dendritic crystals of montebrasite are also contained within K-feldspar (Fig. 1b; Table 1). The crystals are colorless, milky white, or light salmon in color and possess a vitreous luster. The amblygonite–montebrasite series contains various alteration minerals including fluorapatite, crandallite, goyazite, waylandite, wardite, viitaniemiite, morinite, muscovite, lepidolite, and cookeite (Shirose and Uehara 2014). They were associated with lacroixite, quartz, and topaz. Moreover, tantalite-(Mn), microlite, and minor bismuth were observed as inclusions. Furthermore, eight specimens from five localities were used and included the Myokenzan pegmatite, Tanco pegmatite, Varuträsk pegmatite, Havey pegmatite, and Minas Gerais (Table 1). The montebrasite from the Myokenzan pegmatite, Tanco pegmatite,

Varuträsk pegmatite, and Havey pegmatite correspond to the blocky crystals that are colorless, milky white, or light salmon in color (Figs. 1c, d, e; Table 1). The montebrasite from Minas Gerais was clear yellow and transparent (Fig. 1f; Table 1). Examinations using a polarizing microscope indicated that the montebrasite and amblygonite from the Nagatare pegmatite were mostly cloudy owing to very fine inclusions and micro pores (Figs. 2a, b). Polysynthetic twins were also observed in the specimens, and twins like tartan were occasionally formed in the crystals (Fig. 2b). Secondary veined montebrasite with extremely low fluorine contents had a higher interference color (Fig. 2c). This texture was reported by London and Burt (1982) and Shirose and Uehara (2014). The secondary low fluorine montebrasite was formed by hydrothermal alterations. The montebrasite from the Myokenzan pegmatite, Tanco pegmatite, Varuträsk pegmatite, and Havey pegmatite also included fine inclusions and polysynthetic twins as observed under the polarizing microscope. In contrast, the montebrasite from Minas Gerais had clear crystal without fine inclusions and involved no polysynthetic twins (Fig. 2d).

XRD experiment at room temperature

The fluorine contents of the amblygonite–montebrasite series from the Nagatare pegmatite were estimated from bulk powder XRD patterns and corresponded to F/(F+OH) = 0.40–0.59 (Table 1), which was consistent with the common value of the amblygonite–montebrasite series in natural occurrences. The value led to a concentration of 1.4–2.0 wt% fluorine in the pegmatite melt using the partition coefficient for fluorine between the amblygonite–montebrasite series and a pegmatite melt (London et al. 2001). Lacroixite contents of the amblygonite–montebrasite crystals from the Nagatare pegmatite were estimated from powder XRD patterns, and their values were in the range of 0.3–5.8 wt% (Table 1). The lacroixite contents of the amblygonite–montebrasite series positively correlated to the fluorine contents of the amblygonite–montebrasite series (Table 1). The values of F/(F+OH) of the amblygonite–montebrasite series from other localities were in the range of 0.13–0.49, and the lacroixite contents were in the range of 0–6.0 wt% (Table 1).

Chemical analyses and microtextures

The fluorine contents in the amblygonite–montebrasite series as measured by EPMA-WDS

were inhomogeneous, and lower than the value estimated by XRD in a few parts (Tables 1, 2, 3, 4). In particular, secondary veined montebrasite that revealed a higher interference color under the polarization microscope involved extremely low fluorine contents (Fig. 2c; Table 2). The maximum value of fluorine contents in each specimen measured by EPMA-WDS approach the value estimated by XRD (Table 1). The inhomogeneous lower values of fluorine contents were caused by hydrothermal alterations. Sodium, calcium, and iron were not detected in the montebrasite and amblygonite with the exception of the case of fine lacroixite contamination in a few analysis spots. In the EPMA observations of textures, montebrasite and amblygonite from the Nagatare pegmatite were partially replaced by various secondary phosphates, crandallite, goyazite, fluorapatite, wardite, morinite, and viitaniemiite among others and involved a veined texture comprising acicular or platy fine crystals (Shirose and Uehara 2014). However, lacroixite exhibited different textures with patchy areas or lamellae up to 10 μm that were scattered and directionally arranged in montebrasite and amblygonite (Figs. 3a, b). Moreover, lacroixite was contained in all the amblygonite–montebrasite specimens from the Nagatare pegmatite and thereby differed from other Na-phosphates. The patchy lacroixite and secondary minerals correspond to the fine inclusions observed under the polarizing microscope. Secondary

veins of low fluorine montebrasite did not possess any lacroixite inside (Figs. 3c, d), and the veins cut the zone of the amblygonite–montebrasite series with lacroixite (Fig. 3c). The low fluorine montebrasite were occasionally fine subhedral crystals associated fluorapatite (Fig. 3d). The textures indicate that lacroixite was formed by a process that was different from a hydrothermal alteration associated with secondary phosphates. The specimens from the Varuträsk and Havey pegmatites exhibited lacroixite patches similar to the specimens from the Nagatare pegmatite. For the specimens from the Myokenzan and Tanco pegmatites, although lacroixite was not distinguishable by the XRD experiments, it was marginally confirmed by the EPMA observations in only mid fluorine specimens (MY13, MY14, and XS109).

TEM/STEM observation

TEM/STEM analyses were used to observe lacroixite in montebrasite from the Nagatare pegmatite, and it exhibited a bidirectionally developed patchy texture with flat planes on the boundary with montebrasite. Furthermore, lacroixite was associated with low fluorine montebrasite, which also formed nanoscale lamellae within the patch (Figs. 4a, b). The

grain boundaries comprised (1−10) and (110) planes. The former developed between the patches and host montebrasite, whereas the latter developed between the lacroixite and low fluorine montebrasite (Fig. 4b). The selected area electron diffraction (SAED) pattern shows that the crystal orientations of lacroixite and host montebrasite were identical (Fig. 4c). The doublet spots caused by monoclinic lacroixite (γ = 90°) and triclinic host montebrasite (γ > 90°) were observed in the SAED pattern from the [001] direction of montebrasite (Fig. 4c). The crystal orientations of lacroixite and low fluorine montebrasite were also similar, and the triplet spots of lacroixite, low fluorine montebrasite, and host montebrasite were observed (Fig. 4d). Figure 5 shows the X-ray mapping images obtained via STEM-EDS. Qualitative analyses by STEM-EDS revealed that the montebrasite lamellae had negligible fluorine content. Figure 6 shows a high-resolution image of the lacroixite from the [001] direction and crystal structures of montebrasite and lacroixite. (1−10) and (110) planes comprised arranged AlO_6 polyhedral chains along the *c* axis that corresponded to the cleavage planes. TEM/STEM observations indicated crystallographic relationships between patchy lacroixite, patchy low fluorine montebrasite, and host montebrasite.

XRD experiments at high temperature

Changes in unit cell parameters of amblygonite were confirmed in the XRD experiments involving the heating of samples from the Nagatare pegmatite. Increases in temperature resulted in an increase in the *b* axis with a higher slope when compared with those of the *a* and *c* axes with decreases in α, β, and γ values (Fig. 7; Table 5). However, the amblygonite was partially broken down at 600 °C, and anhydrous phosphates were formed. At 700 °C, the amblygonite was completely broken down, and berlinite was formed. The easy breakdown of amblygonite and formation of anhydrous phosphates with increase in temperature was attributed to dehydration in a vacuum dry condition. Experiments in wet condition are required for the validation of properties of the amblygonite–montebrasite series at high temperature. The changes in the unit cell parameters for the montebrasite–amblygonite series at a high temperature was consistent with the behavior at low temperature as indicated by Groat et al. (2003). Due to increases in the temperature, the structure of the amblygonite–montebrasite series was closing to a monoclinic structure such as that of lacroixite. In addition, a high-temperature phase of the amblygonite–montebrasite series and exsolution texture with lacroixite are formed above at least 500 °C.

Discussion

Exsolution process of the amblygonite–montebrasite series and lacroixite

The formation process of lacroixite differs from other secondary phosphates formed by hydrothermal alterations because lacroixite was found in all specimens from the Nagatare pegmatite as scattered patches or lamellae embedded in montebrasite and amblygonite (Fig. 3; Table 1). The texture of the scattered lacroixite was similar to that of the discredited "natromontebrasite" (Fransolet 1989; Fransolet et al. 2007), and it is a typical texture in the amblygonite–montebrasite series. The fact that secondary montebrasite veins did not contain any lacroixite also supports its different formation process from hydrothermal alterations (Figs. 3c, d). TEM/STEM analyses indicated that lacroixite patches with low fluorine montebrasite lamellae had an identical crystal orientation to the host montebrasite (Fig. 4), and they had a crystallographic relationship with each other. As mentioned in Groat et al. (1990), the crystal structure of the amblygonite–montebrasite series is topologically identical to the lacroixite structure, although sodium could not substitute the

lithium in the amblygonite–montebrasite structure. However, the apparent changes in the unit cell parameters of the amblygonite–montebrasite at high temperatures indicate a possibility of the formation of a solid solution at a high temperature, and reductions in the temperature formed the miscibility gap between lacroixite and the amblygonite–montebrasite series and exsolution textures.

Thus, the following exsolution process was estimated. First, a Li-rich high-temperature phase, ((Li,Na)Al(PO_4)(OH,F) with *C*2/*c*) was formed, and then owing to temperature decreases, the phase was exsolved into high amblygonite–montebrasite (LiAl(PO_4)(OH,F) with *C*2/*c*) and lamellae of a mid-temperature phase ((Li,Na)Al(PO_4)(OH,F) with *C*2/*c*) containing approximately the same amounts of lithium and sodium) (Fig. 8). The host phase subsequently transformed to amblygonite–montebrasite (LiAl(PO_4)(OH,F) with *C*−1), and polysynthetic twins were formed in the amblygonite–montebrasite during this transition. Finally, the lamella of the mid-temperature phase was exsolved into low fluorine montebrasite (LiAl(PO_4)(OH) with *C*−1) and lacroixite (NaAl(PO_4)F with *C*2/*c*). As a result, the amblygonite–montebrasite series involved a patchy or lamellar texture as shown in the EPMA and TEM/STEM observations (Figs. 3, 4, 8). For the formation of the high-temperature phase of the

amblygonite–montebrasite series, exceeding the temperature to at least 500 °C based on the results of the high-temperature XRD experiments is necessary (Fig. 7).

The formation of the miscibility gap was caused by the difference in ion radius between Li^+ and Na^+, and it was analogous to the exsolution process of alkali feldspars such as perthite. Fransolet (1989) reported that lacroixite could contain minor Li^+ and OH^- with changes in the unit cell parameters. The change was noticeable in the *b* axis and was similar to that of the amblygonite–montebrasite series under heating conditions in the present study (Fig. 7). The lamellae in TEM/STEM observations comprised low fluorine montebrasite and fluorine-rich lacroixite (Fig. 4), which indicated that the OH^- was suitable for a triclinic structure with Li^+, whereas the F^- was suitable for a monoclinic structure with Na^+ at low temperature (Fig. 8). In addition to the low fluorine environment, a crystallographic restriction caused the low fluorine content of secondary montebrasite formed by a hydrothermal alteration. This was confirmed by the occurrence of low fluorine montebrasite coexisting with fluorapatite or fluorine-rich minerals such as morinite and viitaniemiite (Figs. 3c, d). Though the possibility of exsolution has been emphasized so far, simultaneous intergrowth is also expected to occur in pegmatite-forming conditions like pollucite–analcime solid solution (London 1998). However, the change of grain size along

the growth direction was not indicated in patchy lacroixite from the localities in this study. The rapid crystallization condition in the pegmatite formed dendritic montebrasite (Fig. 1b) although the development of patchy lacroixite was not correlated to the oversaturated conditions in the melt forming the pegmatite. The patchy lacroixite in the amblygonite–montebrasite series from the Nagatare pegmatite was formed by the exsolution process.

Exsolution texture and occurrence condition

The lacroixite contents of the amblygonite–montebrasite series from the Nagatare pegmatite were positively correlated to the fluorine contents (Fig. 9; Table 1), which were controlled by the thermal and chemical environments at pegmatite formation. The lacroixite contents were subdivided into three types, namely high- (5.8–3.3 wt%), mid- (2.7–0.5 wt%), and low-lacroixite (0.3 wt%) types, and they corresponded to large- (60–10 mm), mid- (20–3 mm), and fine-grained (5 mm) amblygonite–montebrasite series, respectively (Fig. 9). In particular, the low-lacroixite type montebrasite exhibited dendritic textures (Fig. 1b), and this indicated that a low-lacroixite type montebrasite was formed in a lower temperature environment with rapid growth under a supercool condition as mentioned by London

(2008). The high-lacroixite type with large grain size was formed with slight undercooling and higher temperature condition. These textures and conditions were consistent with the proposed exsolution process model of the amblygonite–montebrasite series and lacroixite that the amblygonite–montebrasite series formed at high temperature could contain sodium (Fig. 8).

Lacroixite contents of the amblygonite–montebrasite series could be applied to gain an understanding of primary amblygonite–montebrasite series forming conditions. In addition, the exsolution textures and lacroixite could not be present in the amblygonite–montebrasite series formed at low temperature. The formation temperatures of montebrasite and amblygonite from various localities could be roughly estimated from the occurrence of associated Li-aluminosilicate using a phase diagram (London 1984). Low to high lacroixite contents were included in the amblygonite–montebrasite series from the Nagatare pegmatite with petalite as the only Li-aluminosilicate phase, whereas no or low lacroixite were included in the amblygonite–montebrasite series from lower-temperature LCT pegmatites with spodumene as the Myokenzan, Tanco, and Varuträsk pegmatites (Fig, 10). A characteristic property was confirmed for the specimen from Minas Gerais in Brazil wherein the polysynthetic twins and lacroixite were not present in montebrasite (Figs. 1f,

2d). This type of montebrasite involved a gem-quality montebrasite from drusy vugs that was formed at a low temperature near hydrothermal conditions. The specimen also exhibited extremely low fluorine contents (Tables 1, 4) and corresponded to the water-clear gem-quality montebrasite with extremely low fluorine contents reported by Černá et al. (1973) and Rondeau et al. (2006). The low fluorine montebrasite was formed below the exsolution and transformation temperature or under the hydrothermal environments.

The chemical analysis data and lacroixite contents of the amblygonite–montebrasite series in previous studies were also verified based on the exsolution process model. In some former studies, lacroixite was analyzed together with the amblygonite–montebrasite series without recognition, resulting as sodium contents in chemical analysis. Černá et al. (1973) used wet chemical analyses to analyze montebrasite and amblygonite from various localities, and in particular, specimens from the Tanco pegmatite, and indicated that the sodium contents of the amblygonite–montebrasite series had a positive correlation with fluorine contents. However, the amblygonite–montebrasite series did not contain sodium at room temperature, and Groat et al. (1990) confirmed that the sodium-rich specimens (AF-1 and AF-65) investigated by Černá et al. (1973) contained abundant amounts of lacroixite. Therefore, sodium contents of montebrasite and amblygonite

investigated by Černá et al. (1973) could be converted to lacroixite contents. In addition, London et al. (2001) indicated that synthesized montebrasite and amblygonite in haplogranitic melt at 585 °C and 200 MPa of H_2O exhibited positive correlation of sodium and fluorine by EPMA, although natural amblygonite did not contain any detectable sodium. It was considered as a fine lacroixite mixture or high-temperature phase, and it could be converted to lacroixite contents. The converted data set is shown in Figure 11. The positive correlation between lacroixite and fluorine contents was confirmed and consistent with the results of the analyzed specimens in this study (Figs. 10, 11). The quantity of lacroixite in the amblygonite–montebrasite series was restricted by the fluorine contents in addition to formation temperature. High fluorine amblygonite from topaz-bearing granites of Western Europe contained abundant lacroixite (London et al. 2001; Groat et al. 1990), and they were formed under the fluorine-rich environment at the higher temperature. The unit cell parameters of the amblygonite–montebrasite series become close to that of monoclinic structures such as lacroixite with increasing fluorine. Similarly, at high temperature, the fluorine-rich phase prefers sodium owing to monoclinicity. As a result, the lacroixite contents were correlated with the fluorine contents in the amblygonite–montebrasite series (Figs. 10, 11). In conclusion, the amblygonite–montebrasite series had

various amounts of lacroixite and fluorine contents, and their properties were correlated to the thermal and chemical environments at pegmatite formations.

Implications

The results obtained in this study on the amblygonite–montebrasite series from the Nagatare pegmatite revealed that a new microtexture existed in all specimens of subhedral blocky amblygonite–montebrasite and dendritic montebrasite crystals. TEM/STEM analyses were very effective for investigation of micro patches or lamellae in amblygonite and montebrasite hosts, and it revealed that the patches or lamellae had a characteristic microtexture involving nanoscale lamella of lacroixite and a low-fluorine montebrasite. The patchy and lamellar textures are an important evidence of the exsolution process with slow cooling, and a solid solution phase between lacroixite and the amblygonite–montebrasite series at high temperature should be expected in pegmatite-forming process. The texture was not present in some montebrasite from other localities, that is, they were formed at low temperature where a solvus in the lacroixite–amblygonite–montebrasite series would be present. The confirmed diversity of texture in the amblygonite–montebrasite series can be good indicator of pegmatite-forming process. The amblygonite–montebrasite series

generally occurs characteristic to pegmatite-forming granitic melts with high-phosphorus contents, derived from the melting of aluminous metasedimentary rocks (e.g., London et al. 1999). In the overview of phosphates from pegmatites, the possibility of rapid cooling for the formation of skeletal crystals of the amblygonite–montebrasite series was indicated (London 2008, 2017), while he also pointed out that the nature of the growth of phosphate crystals in pegmatites was almost wholly unstudied. Pegmatitic texture is considered as a consequence of delayed nucleation and rapid growth at large undercooling (e.g., Nabelek et al. 2010), and the formation of dendritic amblygonite–montebrasite series was also considered as the result of rapid cooling. So two stages of cooling could be indicated from this macro and micro textures, where dendritic crystals rapidly crystallized followed by the development of micro lamellae during slow cooling.

The variety of texture of the amblygonite–montebrasite series indicated in this study provided new interpretations to the various chemical compositions of the amblygonite–montebrasite series analyzed by Černá et al. (1973). Low-fluorine montebrasite without exsolution texture from miarolitic cavity was formed in the magmatic–hydrothermal transition at a low temperature. “Natromontebrasite”, with an intergrowth of lacroixite within the amblygonite–montebrasite series proved by Fransolet

(1989) and Fransolet et al. (2007), occurred as exsolution products from a high temperature phase. The amblygonite–montebrasite series, enriched in fluxing components such as Li, P, F, and OH, provides important clue to the crystallization of fluxing components in pegmatite-forming melts. In the recent model of pegmatite-forming processes, flux-rich boundary layer in pegmatite-forming melts has important role for giant crystal formation and rare-elements enrichment in pegmatite (e.g., London 2014). Quantification of forming condition requires additional microtexture investigation of the amblygonite–montebrasite series from other localities, involving observations of the lamellar shape, size, and distribution. Synthetic experiments of the lacroixite–amblygonite–montebrasite series and the microtexture observation of the synthetic products for determination of the solvus temperature could establish more quantitative restrictions and provide precise information of thermal and chemical changes in pegmatite.

Acknowledgements: We appreciate K. Watanabe for supplying specimens (MY13, 14). We are grateful to D. London for handling the manuscript and many constructive comments. We sincerely thank P. Vignola and an anonymous reviewer for their constructive and critical comments on this manuscript. This work was supported by JSPS KAKENHI Grant

Number 14J03404. The authors thank the Professor Matsumoto Scholarship Fund.

References

Baldwin, J.R., Hill, P.G., von Knorring, O., and Oliver, G.J.H. (2000) Exotic aluminum phosphates, natromontebrasite, brazilianite, goyazite, gorceixite and crandallite from rare-element pegmatites in Namibia. Mineralogical Magazine, 64, 1147–1164.

Černá, I., Černý, P., and Ferguson, R.B. (1973) The fluorine content and some physical properties of the amblygonite–montebrasite minerals. American Mineralogist, 58, 291–301.

Černý, P., and Ercit, T.S. (2005) The classification of granitic pegmatites revisited. Canadian Mineralogist, 43, 2005–2026.

Fransolet, A.M. (1989) The problem of Na–Li substitution in primary Li–Al phosphates: new data on lacroixite, a relatively widespread mineral. Canadian Mineralogist, 27, 211–217.

Fransolet, A.M., Fontan, F., and de Parseval, P. (2007) Natromontebrasite, a discredited mineral species. Canadian Mineralogist, 45, 391–396.

Galliski, M.Á., Černý, P., Márquez–Zavalía, M.F., and Chapman, R. (2012) An association of secondary Al–Li–Be–Ca–Sr phosphates in the San Elías pegmatite, San Luis, Argentina. Canadian Mineralogist, 50, 933–942.

Greiner, D.J., and Bloss, F.D. (1987) Amblygonite–montebrasite optics: Response to (OH^-) orientation and rapid estimation of F from 2*V*. American Mineralogist, 72, 617–624.

Groat, L.A., Raudsepp, M., Hawthorne, F.C., Ercit, T.S., Sherriff, B.L., and Hartman, J.S. (1990) The amblygonite–montebrasite series: Characterization by single-crystal structure refinement, infrared spectroscopy, and multinuclear MAS–NMR spectroscopy. American Mineralogist, 75, 992–1008.

Groat, L.A., Chakoumakos, B.C., Brouwer, D.H., Hoffman, C.M., Fyfe, C.A., Morell, H., and Schultz, A.J. (2003) The amblygonite ($LiAlPO_4F$)–montebrasite ($LiAlPO_4OH$) solid solution: A combined powder and single-crystal neutron diffraction and solid-state 6Li MAS, CP MAS, and REDOR NMR study. American Mineralogist, 88, 195–210.

Kallio, P. (1978) A new X-ray method for the estimation of fluorine content in montebrasites. American Mineralogist, 63, 1249–1251.

Karakida, Y., Tomita, S., Shimoyama, S., and Chijiwa, K. (1994) Geology of the Fukuoka district, Geological Sheet Map 1:50,000, Fukuoka (14) No. 51, 192 p. Geological Survey of Japan, Tokyo (in Japanese with English abstract).

Kataoka, Y., and Uehara, S. (2000) Lepidolite in a lithium pegmatite from Nagatare, Fukuoka Prefecture, Japan. Proceedings of 2000 Annual Meeting of the Mineralogical Society of Japan, p. 101. Mineralogical Society of Japan (in Japanese).

Kuwano, N., and Hikita, T. (1967) Montebrasite from Nagatare, Fukuoka, Japan. Chigaku Kenkyuu (Present "Journal of Geoscience"), 18, 243–245 (in Japanese).

London, D. (1984) Experimental phase equilibria in the system $LiAlSiO_4$–SiO_2–H_2O: A petrogenetic grid for lithium-rich pegmatites. American Mineralogist, 69, 995–1004.

London, D. (2008) Pegmatites. The Canadian Mineralogist Special Publication, 10, 368.

London, D. (2014) A petrologic assessment of internal zonation in granitic pegmatites. Lithos, 184-187, 74-104.

London, D. (2017) Reading pegmatites: What lithium minerals say. Rocks & Minerals, 92, 144-157.

London, D., and Burt, D.M. (1982) Alteration of spodumene, montebrasite and lithiophilite in pegmatites of the White Picacho District, Arizona. American Mineralogist, 67, 97–

113.

London, D., Morgan, G.B.VI., and Icenhower, J. (1998) Stability and solubility of pollucite in the granite system at 200 MPa H_2O. Canadian Mineralogist, 36, 497–510.

London, D., Wolf, M.B., Morgan, G.B.VI, and Gallego Garrido, M. (1999) Experimental silicate-phosphate equilibria in peraluminous granitic magmas, with a case study of the Alburquerque batholith at Tres Arroyos, Badajoz, Spain. Journal of Petrology, 40, 215-240.

London, D., Morgan, G.B.VI., and Wolf, M.B. (2001) Amblygonite–montebrasite solid solution as monitors of fluorine in evolved granitic and pegmatite melts. American Mineralogist, 86, 225–233.

Nabelek, P.I., Whittington, A.G., and Sirbescu, M.C. (2010) The role of H_2O in rapid emplacement and crystallization of granite pegmatites: Resolving the paradox of large crystals in highly undercooled melts. Contributions to Mineralogy and Petrology, 160, 313–325.

Pajunen, A., and Lathi, S.I. (1985) New data on lacroixite, $NaAlFPO_4$. Part II. Crystal structure. American Mineralogist, 70, 849–855.

Rondeau, B., Fritsch, E., Lefevre, P., Guiraud, M., Fransolet, A.M., and Lulzac, Y. (2006) A

Raman investigation of the amblygonite-montebrasite series. Canadian Mineralogist, 44, 1109–1117.

Shibata, H. (1934) A lithium pegmatite from Nagatare, Imajyuku, Itoshima, Fukuoka Prefecture, Japan. Journal of the Geological Society Japan, 41, 582–603 (in Japanese).

Shirose, Y., and Uehara, S. (2013) Li tourmaline from Nagatare, Fukuoka Prefecture, Japan. Journal of Mineralogical and Petrological Sciences, 108, 238–243.

Shirose, Y., and Uehara, S. (2014) Secondary phosphates in montebrasite and amblygonite from Nagatare, Fukuoka Prefecture, Japan. Journal of Mineralogical and Petrological Sciences, 109, 103–108.

Uehara, S., and Shirose, Y. (2013) Namibite and hechtsbergite from the Nagatare mine, Fukuoka Prefecture, Japan. Journal of Mineralogical and Petrological Sciences, 108, 105–110.

Figure captions

Figure 1. Appearance and optical photo micrograph of montebrasite and amblygonite. (**a**) Subhedral amblygonite from the Nagatare pegmatite (sample XN163). (**b**) Dendritic

montebrasite in K-feldspar from the Nagatare pegmatite (sample Ng104). (**c**) Large blocky montebrasite with quartz from the Myokenzan pegmatite (sample MY12). (**d**) Small subhedral montebrasite in lepidolite and quartz from the Myokenzan pegmatite (sample MY14). (**e**) Subhedral blocky montebrasite from the Tanco pegmatite (sample XS109). (**f**) Transparent montebrasite from Minas Gerais (sample XS110). Amb: amblygonite, Qtz: quartz, Mbr: montebrasite, kfs: K-feldspar, Lpd: lepidolite.

Figure 2. (**a**) Plane-polarized optical photomicrographs of montebrasite that show the cloudy parts and developed cracks (sample XN164). (**b**) Cross-polarized optical photomicrographs of montebrasite that show the lattice-shaped polysynthetic twins of montebrasite (sample XN164). (**c**) Cross-polarized optical photomicrographs of the amblygonite–montebrasite series with a vein of secondary low fluorine montebrasite along a fracture (sample XN163). Amb–Mbr: amblygonite–montebrasite series, Mbr^2: secondary montebrasite. (**d**) Cross-polarized optical photomicrographs of montebrasite that did not show any polysynthetic twins or cloudy parts (sample XS110).

Figure 3. Backscattered electron (BSE) images of internal textures in the montebrasite and

amblygonite from the Nagatare pegmatite. (**a**) Scattered lacroixite embedded in montebrasite (sample Ng107). (**b**) Enlargement of Fig. 3a. The lacroixite exhibits a patchy texture. (**c**) The vein of secondary low fluorine montebrasite along a fracture did not contain any lacroixite inside (sample XN164). (**d**) Subhedral fine grains of secondary low fluorine montebrasite with fluorapatite without lacroixite (sample XN165). Lcx: lacroixite, Mbr: montebrasite, Mbr^2: secondary montebrasite, and Fap: fluorapatite.

Figure 4. Scanning transmission electron microscope (STEM) bright field/high angle annular dark field (BF/HAADF) images of the lacroixite patch and selected area electron diffraction (SAED) patterns (sample Ng104). (**a**) STEM BF image from $[001]_{Mbr}$. (**b**) STEM HAADF image of the same area as shown in Fig. 4a. Lacroixite exhibits a bidirectionally developed patch texture with flat planes on the boundary with montebrasite, and the lacroixite is associated with low fluorine montebrasite. Boundary planes comprise (110) and highly developed (1−10) planes. (**c**) SAED patterns from the circle area in Fig. 4b. Patchy lacroixite and host montebrasite exhibited identical crystal orientations. The enlarged image shows the splitting of the spots owing to the difference in unit cell parameters. (**d**) SAED patterns of lacroixite, low fluorine montebrasite, and host

montebrasite. The enlarged image shows the triple spots. Mbr: montebrasite, Lcx: lacroixite, Low-F Mbr: low fluorine montebrasite.

Figure 5. X-ray images of element distribution map (BF image, P*K*α, Al*K*α, Na*K*α, F*K*α, and overlay image of Na*K*α and F*K*α).

Figure 6. Crystal structures of montebrasite and lacroixite from the [001] direction and high-resolution image of lacroixite from the [001] direction. Crystal structure data are based on Groat et al. (2003) and Pajunen and Lathi (1985). The amblygonite–montebrasite series is topologically identical to the lacroixite structure. In addition, the (110) and (1−10) planes comprise arranged AlO_6 polyhedral chains along the *c* axis, and they correspond to the cleavage planes.

Figure 7. Changes in unit cell parameters of the amblygonite–montebrasite series. The amblygonite specimen is heated from 50 °C to 700 °C and the X-ray diffraction (XRD) patterns are measured in situ (sample XN163). The unit cell parameters are listed in Table 5. Data at low temperatures are based on Groat et al. (2003). The bars indicate standard

deviations.

Figure 8. Schematic of an exsolution process model in the amblygonite–montebrasite series. The right column indicates a change in textures. The dashed lines in the texture models represent the formation of polysynthetic twins.

Figure 9. Fluorine contents (apfu) vs. lacroixite contents (wt%) of montebrasite and amblygonite from the Nagatare pegmatite as estimated by the XRD patterns. The values on symbols correspond to grain size. The bars indicate standard deviations.

Figure 10. Fluorine contents (apfu) vs. lacroixite contents (wt%) of montebrasite and amblygonite as estimated by the XRD patterns in the study. The detailed properties are listed in Table 1. The colors of the symbols correspond to the formation environment; that is, orange: petalite occurrence, bicolor: petalite and spodumene occurrence, yellow: spodumene occurrence, gray: no aluminosilicate or uncertain, and light blue: in cavity. The bars indicate standard deviations.

Figure 11. Fluorine contents (apfu) vs. lacroixite contents (wt%) of montebrasite and amblygonite as shown in previous studies. The lacroixite contents are converted from the Na_2O contents of montebrasite and amblygonite. The data are based on chemical analyses of montebrasite and amblygonite from various localities (Černá et al. 1973) and montebrasite and amblygonite synthesized at 585 °C and 200 MPa of H_2O (London et al. 2001). Colors of symbols are the same as those in Fig. 10.

Table 1. Mineralogical properties of montebrasite and amblygonite specimens.

Sample no.	Size (cm)	Habit	Color	Associated minerals[a]	F contents (*apfu*)			Lacroixite[c] contents (wt%)
					XRD[b]	EPMA		
						Av.	Range	
				Nagatare pegmatite, Japan				
XN162	6	Blocky	LS-CL-MW	Qtz, Lpd, Ab	0.58	0.38	0.26–0.51	5.8 (7)
XN165	2	Blocky	LS-MW	Ab, Qtz	0.55	0.23	0.08–0.42	2.7 (5)
XN163	4	Blocky	CL-LS-MW	Qtz	0.54	0.47	0.39–0.50	4.8 (5)
XN160	4	Blocky	CL-MW	(Qtz, Lpd, Ab)	0.53	0.50	0.46–0.56	4.8 (11)
XN168	0.5	Dendritic	LS-CL-MW	Kfs, Qtz, Lpd, Ab, (Tur)	0.49	0.34	0.20–0.40	2.2 (3)
XN167	0.3	Blocky	CL-MW	Qtz, Lpd, Ab, Kfs, Tur	0.47	0.42	0.28–0.52	1.9 (2)
Ng104	0.5	Dendritic	CL-MW	Kfs, Qtz, Lpd, (Ab, Tur)	0.47	0.40	0.32–0.45	0.3 (2)
XN169	1	Blocky	LS-MW	Ab, (Qtz, Lpd)	0.46	0.39	0.22–0.51	3.8 (3)
Ng107	4	Blocky	MW	(Qtz, Lpd)	0.44	0.20	0.17–0.23	3.3 (11)
XN164	2	Blocky	LS-MW	Ab, Ptl, (Lpd)	0.40	0.41	0.26–0.60	3.6 (7)
XN166	2	Blocky	MW	Qtz, Lpd-Ms, (Ab)	0.40	0.30	0.27–0.32	0.5 (2)
				Myokenzan pegmatite, Japan				
MY14	0.6	Blocky	MW-CL	Lpd, Qtz, Ab	0.42	0.40	0.33–0.48	0.0[d]
MY13	1	Blocky	LS-MW	Ab, (Tur, Qtz, Lpd)	0.36	0.24	0.14–0.38	0.0[d]
MY12	10	Blocky	CL-MW	Qtz	0.25	0.18	0.14–0.23	N.D.
MY11	10	Blocky	CL-MW	Ab, Qtz	0.18	0.15	0.10–0.17	N.D.
				Tanco pegmatite, Canada				
XS109	6	Blocky	MW	-	0.49	0.35	0.12–0.40	0.0[d]
				Varuträsk pegmatite, Sweden				
XS113	12	Blocky	CL-MW	-	0.40	0.37	0.27–0.42	1.1 (3)
				Havey pegmatite, U.S.A.				
XS112	12	Blocky	MW	Ab, Qtz	0.29	0.31	0.16–0.39	6.0 (3)
				Minas Gerais, Brazil				
XS110	2	Blocky	CY	-	0.13	0.14	0.12–0.17	N.D.

Notes: LS: light salmon color, CL: colorless, MW: milky white color, CY: clear yellow color. Qtz: quartz, Lpd: lepidolite, The specimens used from the Nagatare pegmatite (XN, Ng) are same as the specimens used by Shirose and Uehara

[a] Slightly associated minerals are noted in brackets.

[b] F contents were estimated from bulk powder XRD of montebrasite and amblygonite crystals for all the specimens us

[c] The value in brackets means analytical error.

[d] Lacroixite was not detected by XRD, and marginally confirmed by EPMA observations.

Ab: albite, Kfs: K-feldspar, Tur: Li tourmaline, Ptl: petalite, Ms: muscovite, Av.: average value, N.D.: not detectec
(2014). The localities of the other specimens used include the following: Myokenzan pegmatite (Ibaraki Prefecture, Japan (MY)

ing Kallio's (1978) method

), Tanco pegmatite (Manitoba, Canada (XS109); Minas Gerais Brazil (XS110)), Havey pegmatite (Maine, U.S.A. (XS112)), and

Varuträsk pegmatite (Västerbotten, Sweden (XS113

Table 2. Representative chemical composition of amblygonite, montebrasite, secondary low fluorine montebrasite, and l

Species	**Amblygonite**	**Amblygonite**	**Montebrasite**	**Montebrasite**	**Low-F montebrasite**	**Low-F montebrasite**	**Lacroixite** (n = 2)
Sample no.	XN160	XN162	Ng104	XN166	XN164	XN165	XN163
P_2O_5	47.72	48.64	48.96	48.33	48.88	48.16	45.53 (2)
Al_2O_3	34.53	35.89	35.41	34.61	34.78	35.04	29.42 (0)
CaO	0.00	0.00	0.00	0.02	0.00	0.03	0.38 (3)
FeO	0.01	0.02	0.00	0.00	0.00	0.00	
Li_2O*	10.07	10.34	10.33	10.16	10.25	10.19	
Na_2O	0.00	0.00	0.00	0.00	0.00	0.01	16.76 (3)
F	7.12	6.67	5.11	3.84	3.40	1.36	10.38 (3)
H_2O*	2.70	3.07	3.81	4.31	4.57	5.50	0.58
O=F	3.00	2.81	2.15	1.62	1.43	0.57	4.37
Total	99.15	101.83	101.48	99.64	100.45	99.71	98.68
Based on 5 anions pfu, O = 4, F + OH = 1							
P	1.00	0.99	1.00	1.00	1.00	0.99	1.05 (0)
Al	1.00	1.02	1.00	1.00	0.99	1.01	0.95 (1)
Ca	0.00	0.00	0.00	0.00	0.00	0.00	0.01 (1)
Fe	0.00	0.00	0.00	0.00	0.00	0.00	
Li	1.00	1.00	1.00	1.00	1.00	1.00	
Na	0.00	0.00	0.00	0.00	0.00	0.00	0.89 (1)
F	0.56	0.51	0.39	0.30	0.26	0.10	0.90 (2)
OH	0.44	0.49	0.61	0.70	0.74	0.90	0.10 (2)
Cation sum	3.00	3.01	3.00	3.00	3.00	3.00	2.89

Note: Li_2O and H_2O contents were calculated by stoichiometry. The value in brackets means standard deviation.

acroixite from the Nagatare pegmatite as obtained by EPMA analyses.

Table 3. Average chemical composition of amblygonite and montebrasite from the Nagatare pegmatite as indicated by E

Sample no.	**XN162**		**XN165**		**XN163**		**XN160**		**XN168**		**XN167**		**Ng104**	
n	25		22		12		14		21		19		19	
P_2O_5	48.62	(38)	48.13	(47)	48.01	(53)	48.00	(65)	48.78	(33)	48.46	(42)	48.62	(38)
Al_2O_3	35.12	(57)	34.84	(32)	35.00	(29)	34.90	(49)	35.14	(40)	35.59	(31)	35.12	(46)
CaO	0.02	(2)	0.02	(2)	0.02	(2)	0.01	(2)	0.03	(3)	0.02	(2)	0.01	(2)
FeO	0.02	(2)	0.01	(2)	0.01	(1)	0.01	(3)	0.02	(2)	0.01	(2)	0.01	(2)
Li_2O*	10.26	(9)	10.17	(7)	10.17	(9)	10.15	(10)	10.29	(6)	10.29	(6)	10.26	(8)
Na_2O	0.02	(5)	0.05	(10)	0.03	(3)	0.02	(5)	0.07	(8)	0.02	(3)	0.01	(2)
F	5.01	(120)	2.96	(127)	6.02	(38)	6.49	(37)	4.47	(75)	5.45	(85)	5.27	(39)
H_2O*	3.81	(54)	4.73	(60)	3.28	(19)	3.04	(20)	4.08	(35)	3.62	(39)	3.69	(19)
O=F	2.11	(50)	1.25	(53)	2.53	(16)	2.73	(16)	1.88	(31)	2.30	(36)	2.22	(17)
Total	100.77		99.65		100.01		99.90		100.99		101.18		100.77	
									Based on 5 anions pfu, O = 4, F + OH = 1					
P	1.00	(1)	1.00	(1)	0.99	(0)	1.00	(1)	1.00	(0)	0.99	(1)	1.00	(1)
Al	1.00	(1)	1.00	(1)	1.01	(1)	1.01	(1)	1.00	(1)	1.01	(1)	1.00	(1)
Ca	0.00	(0)	0.00	(0)	0.00	(0)	0.00	(0)	0.00	(0)	0.00	(0)	0.00	(0)
Fe	0.00	(0)	0.00	(0)	0.00	(0)	0.00	(0)	0.00	(0)	0.00	(0)	0.00	(0)
Li	1.00		1.00		1.00		1.00		1.00		1.00		1.00	
Na	0.00	(0)	0.00	(1)	0.00	(0)	0.00	(0)	0.00	(0)	0.00	(0)	0.00	(0)
F	0.38	(9)	0.23	(10)	0.47	(3)	0.50	(3)	0.34	(6)	0.42	(6)	0.40	(3)
OH	0.62	(9)	0.77	(10)	0.53	(3)	0.50	(3)	0.66	(6)	0.58	(6)	0.60	(3)
Cation sum	3.00		3.00		3.01		3.00		3.00		3.01		3.00	

Note: Li_2O and H_2O contents were calculated by stoichiometry. The value in brackets means standard deviation.

EPMA analyses.

XN169		Ng107		XN164		XN166	
16		14		23		13	
48.11	(45)	48.09	(41)	48.55	(40)	48.21	(27)
35.35	(41)	34.99	(42)	35.17	(31)	34.90	(28)
0.01	(2)	0.02	(2)	0.02	(3)	0.02	(2)
0.00	(1)	0.02	(2)	0.02	(2)	0.01	(1)
10.22	(9)	10.17	(8)	10.26	(7)	10.18	(6)
0.03	(4)	0.00	(0)	0.09	(12)	0.01	(1)
5.12	(93)	2.64	(21)	5.36	(147)	3.82	(17)
3.74	(44)	4.88	(11)	3.64	(69)	4.33	(8)
2.15	(39)	1.11	(9)	2.26	(62)	1.61	(7)
100.43		99.70		100.86		99.87	
0.99	(0)	0.99	(1)	1.00	(0)	1.00	(0)
1.01	(1)	1.01	(1)	1.00	(1)	1.00	(0)
0.00	(0)	0.00	(0)	0.00	(0)	0.00	(0)
0.00	(0)	0.00	(0)	0.00	(0)	0.00	(0)
1.00		1.00		1.00		1.00	
0.00	(0)	0.00	(0)	0.00	(1)	0.00	(0)
0.39	(7)	0.20	(2)	0.41	(11)	0.30	(1)
0.61	(7)	0.80	(2)	0.59	(11)	0.70	(1)
3.01		3.00		3.01		3.00	

Table 4. Average chemical composition of the amblygonite and montebrasite (from the Myokenzan, Tanco, Minas Gerais

Sample no.	**MY14**		**MY13**		**MY12**		**MY11**		**XS109**		**XS113**		**XS112**		**XS110**	
n	22		22		19		11		16		31		15		14	
P_2O_5	47.95	(47)	47.68	(39)	48.78	(50)	48.63	(36)	48.23	(39)	48.52	(58)	48.52	(44)	48.02	(35)
Al_2O_3	33.83	(31)	33.60	(36)	34.63	(57)	34.75	(36)	34.83	(42)	34.50	(40)	34.47	(48)	34.97	(38)
CaO	0.02	(3)	0.03	(3)	0.02	(2)	0.02	(2)	0.01	(2)	0.02	(2)	0.03	(3)	0.01	(2)
FeO	0.02	(2)	0.02	(3)	0.02	(2)	0.01	(2)	0.02	(2)	0.01	(2)	0.03	(3)	0.03	(3)
Li_2O^a	10.03	(8)	9.97	(7)	10.23	(12)	10.22	(7)	10.17	(8)	10.18	(9)	10.18	(8)	10.16	(7)
Na_2O	0.01	(4)	0.00	(0)	0.00	(0)	0.00	(1)	0.00	(0)	0.05	(24)	0.02	(3)	0.00	(1)
F	5.06	(41)	3.08	(92)	2.38	(32)	1.94	(27)	4.53	(81)	4.75	(101)	4.01	(90)	1.86	(18)
H_2O^a	3.65	(21)	4.55	(44)	5.04	(16)	5.24	(13)	3.99	(37)	3.89	(48)	4.23	(40)	5.25	(8)
O=F	2.13	(17)	1.30	(39)	1.00	(13)	0.82	(11)	1.91	(34)	2.00	(43)	1.69	(38)	0.78	(7)
Total	98.45		97.63		100.09		100.00		99.87		99.92		99.79		99.53	
Based on 5 anions pfu, O = 4, F + OH = 1																
P	1.01	(0)	1.01	(0)	1.00	(0)	1.00	(0)	1.00	(0)	1.00	(1)	1.00	(1)	0.99	(0)
Al	0.99	(1)	0.99	(1)	0.99	(1)	1.00	(1)	1.00	(1)	0.99	(1)	0.99	(1)	1.01	(1)
Ca	0.00	(0)	0.00	(0)	0.00	(0)	0.00	(0)	0.00	(0)	0.00	(0)	0.00	(0)	0.00	(0)
Fe	0.00	(0)	0.00	(0)	0.00	(0)	0.00	(0)	0.00	(0)	0.00	(0)	0.00	(0)	0.00	(0)
Li	1.00		1.00		1.00		1.00		1.00		1.00		1.00		1.00	
Na	0.00	(0)	0.00	(0)	0.00	(0)	0.00	(0)	0.00	(0)	0.00	(1)	0.00	(0)	0.00	(0)
F	0.40	(3)	0.24	(7)	0.18	(2)	0.15	(2)	0.35	(6)	0.37	(8)	0.31	(7)	0.14	(1)
OH	0.60	(3)	0.76	(7)	0.82	(2)	0.85	(2)	0.65	(6)	0.63	(8)	0.69	(7)	0.86	(1)
Cation sum	3.00		3.00		3.00		3.00		3.00		3.00		3.00		3.00	

Note: Myokenzan pegmatite (Ibaraki Prefecture, Japan (MY); Tanco pegmatite, Manitoba, Canada (XS109); Minas Gerai
[a]Li_2O and H_2O contents were calculated by stoichiometry.

) and Varuträsk pegmatites by EPMA analyses

XS114
17
48.88 (43)
34.38 (27)
0.03 (3)
0.02 (3)
10.21 (6)
0.01 (2)
1.07 (57)
5.65 (28)
0.45 (24)
99.80
1.01 (0)
0.99 (1)
0.00 (0)
0.00 (0)
1.00
0.00 (0)
0.08 (4)
0.92 (4)
3.00

s, Brazil (XS110)), Havey pegmatite (Maine, U.S.A. (XS112)), Varuträsk pegmatite (Västerbotten, Sweden (XS113

3)). The value in brackets means standard deviatio

Table 5. Unit cell parameters of the amblygonite specimen (sample XN163) heated from 50°C to 700 °C

	Temp. (°C)	***a*** **(Å)**		***b*** **(Å)**		***c*** **(Å)**		***α*** **(°)**		***β*** **(°)**		***γ*** **(°)**		***V*** **(Å^3)**
Run1	50	6.689	(4)	7.739	(5)	6.968	(5)	90.85	(2)	117.65	(2)	91.27	(2)	319.3
	100	6.694	(4)	7.745	(5)	6.973	(5)	90.84	(2)	117.65	(2)	91.25	(2)	320.0
	200	6.698	(6)	7.750	(8)	6.978	(7)	90.84	(3)	117.62	(3)	91.23	(3)	320.7
	400	6.702	(5)	7.781	(6)	6.992	(5)	90.74	(2)	117.50	(2)	91.14	(2)	323.3
	600	6.712	(9)	7.812	(11)	7.006	(9)	90.68	(4)	117.34	(4)	91.03	(4)	326.2
Run2	50	6.692	(5)	7.731	(7)	6.972	(6)	90.83	(2)	117.69	(2)	91.29	(3)	319.2
	500	6.713	(7)	7.796	(8)	7.004	(7)	90.70	(3)	117.45	(3)	91.12	(3)	325.1
	500	6.716	(10)	7.799	(12)	7.006	(10)	90.72	(5)	117.45	(4)	91.15	(5)	325.5
	500	6.713	(6)	7.800	(8)	7.008	(7)	90.77	(3)	117.45	(3)	91.08	(3)	325.5
	500	6.714	(6)	7.797	(7)	7.006	(6)	90.71	(3)	117.46	(3)	91.10	(3)	325.3
Run3	50	6.692	(6)	7.738	(7)	6.973	(6)	90.85	(3)	117.67	(2)	91.26	(3)	319.6
	600	6.719	(9)	7.806	(11)	7.015	(9)	90.78	(5)	117.42	(4)	91.00	(4)	326.4
	600	6.723	(8)	7.813	(9)	7.008	(8)	90.59	(4)	117.40	(3)	91.08	(3)	326.7

Note: The value in brackets means standard deviation.

(4)
(4)
(5)
(4)
(7)
(5)
(6)
(8)
(6)
(5)
(5)
(8)
(7)

This is a preprint, the final version is subject to change, of the American Mineralogist (MSA)
Cite as Authors (Year) Title. American Mineralogist, in press.
DOI: http://dx.doi.org/10.2138/am-2018-6049

Figure 1

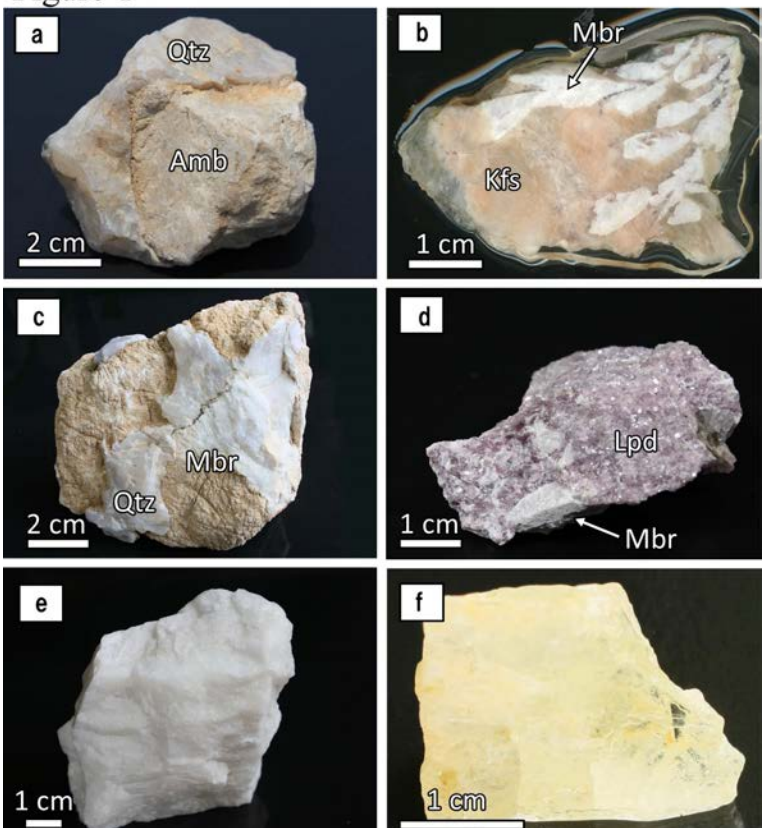

This is a preprint, the final version is subject to change, of the American Mineralogist (MSA)
Cite as Authors (Year) Title. American Mineralogist, in press.
DOI: http://dx.doi.org/10.2138/am-2018-6049

Figure 2

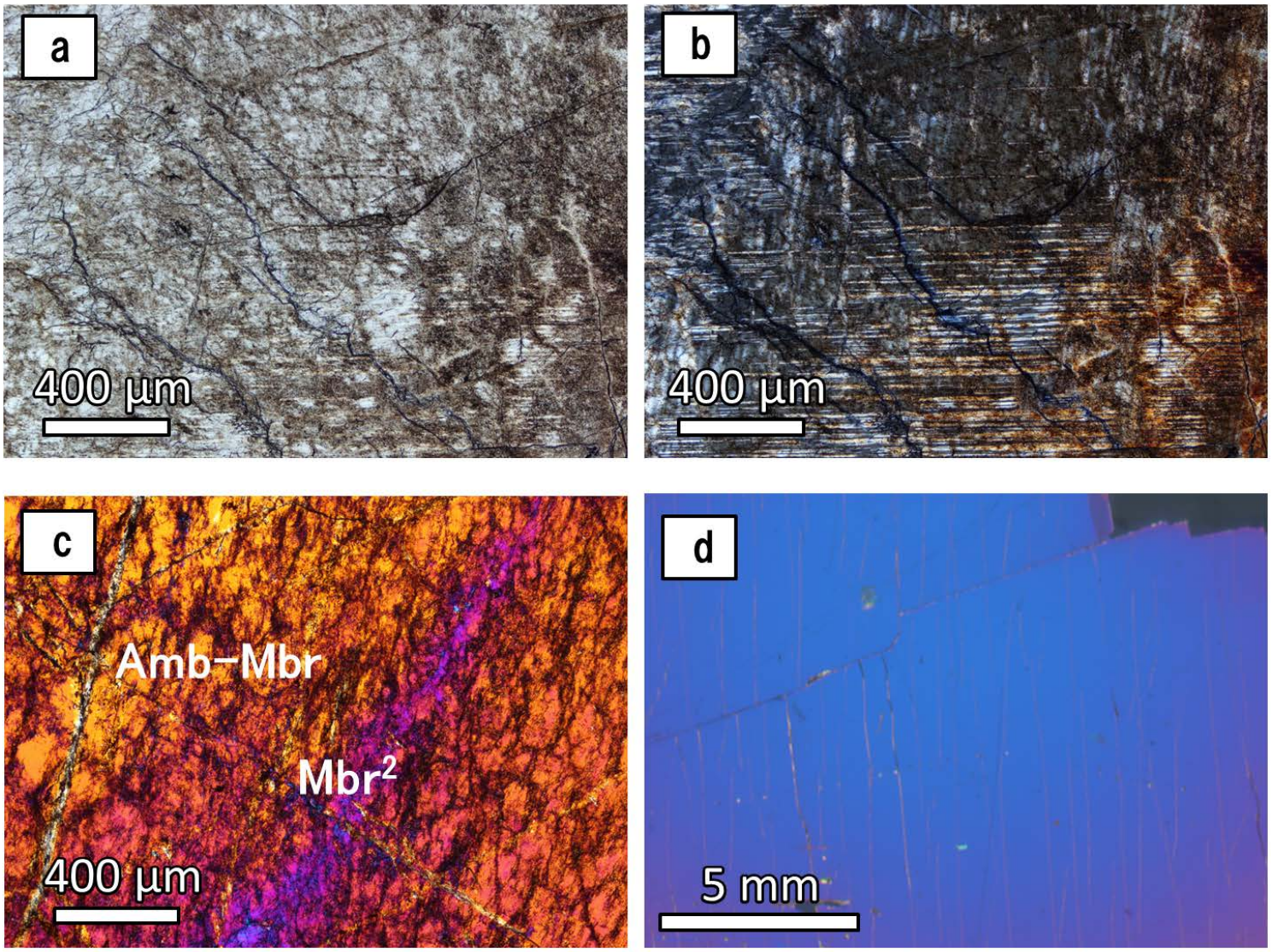

This is a preprint, the final version is subject to change, of the American Mineralogist (MSA)
Cite as Authors (Year) Title. American Mineralogist, in press.
DOI: http://dx.doi.org/10.2138/am-2018-6049

Figure 3

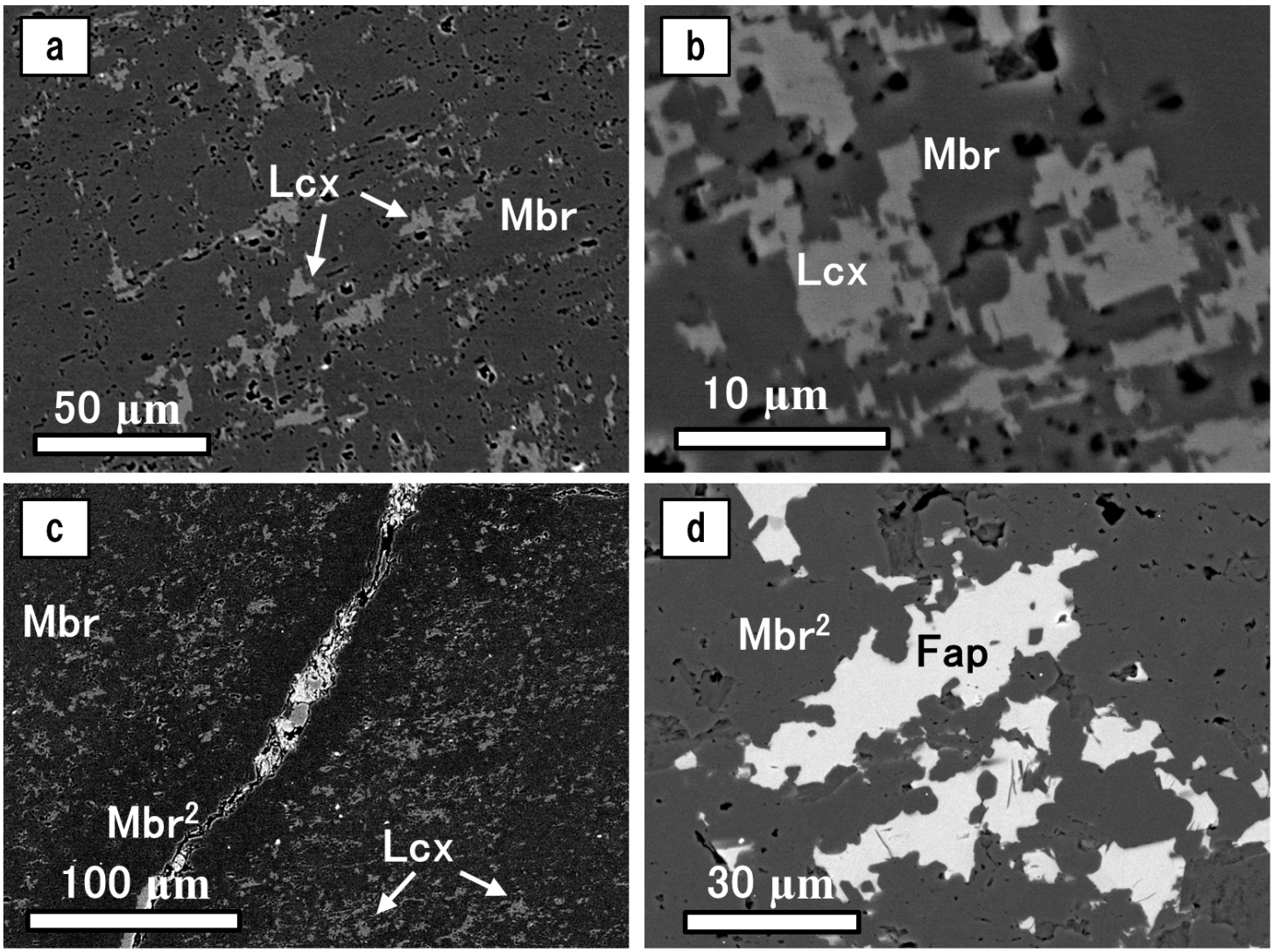

This is a preprint, the final version is subject to change, of the American Mineralogist (MSA)
Cite as Authors (Year) Title. American Mineralogist, in press.
DOI: http://dx.doi.org/10.2138/am-2018-6049

Figure 4

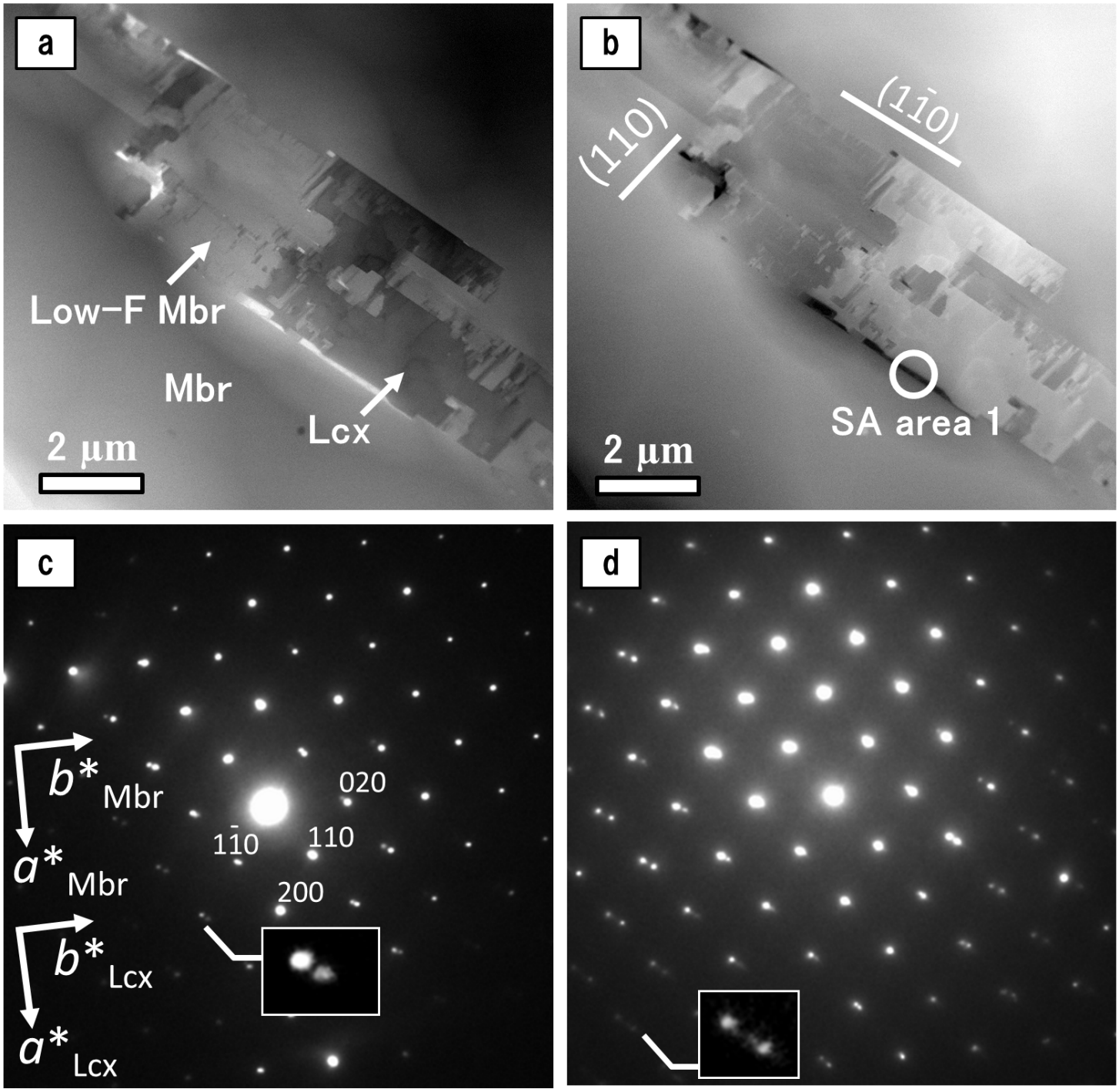

This is a preprint, the final version is subject to change, of the American Mineralogist (MSA)
Cite as Authors (Year) Title. American Mineralogist, in press.
DOI: http://dx.doi.org/10.2138/am-2018-6049

Figure 5

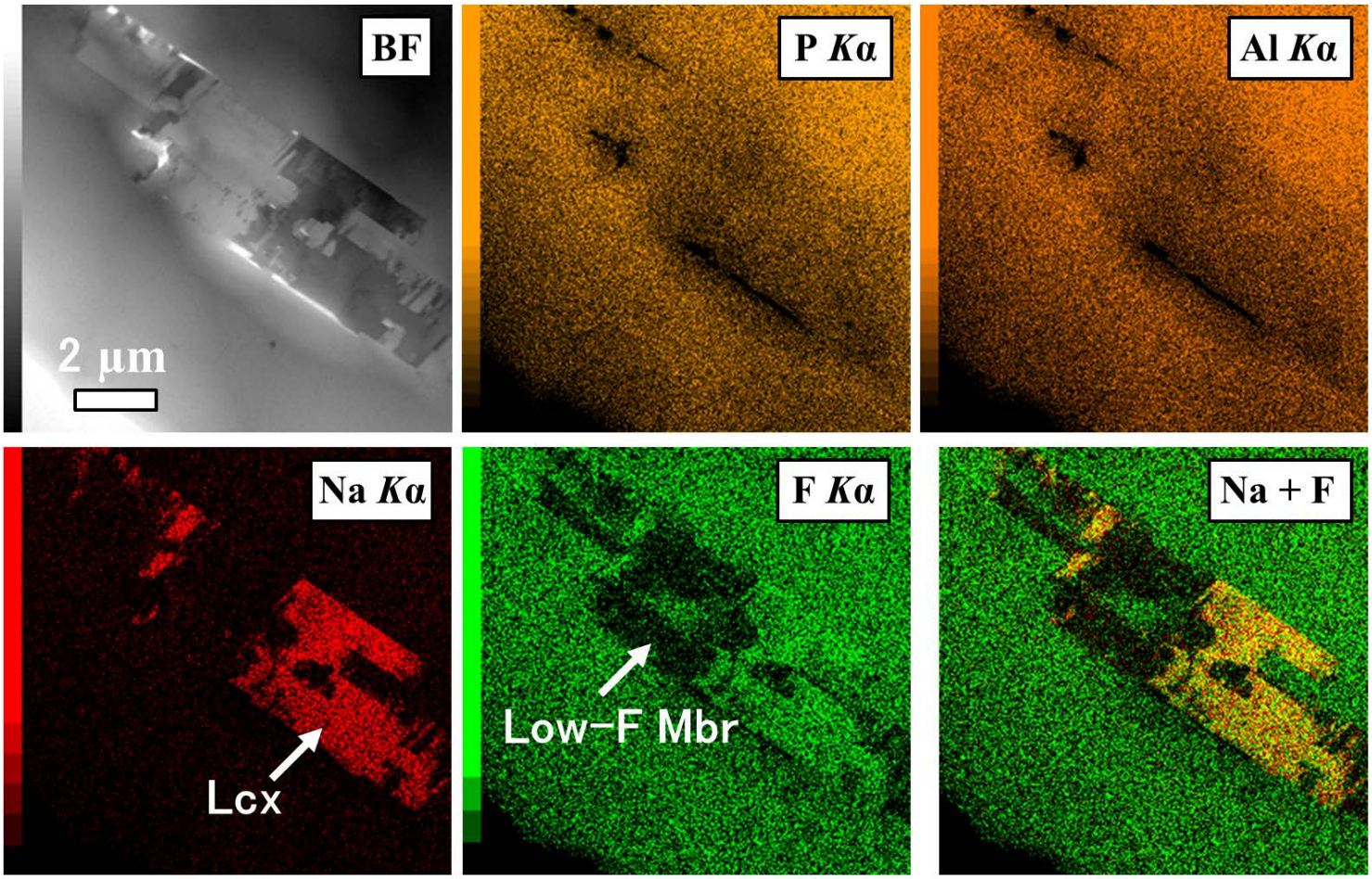

This is a preprint, the final version is subject to change, of the American Mineralogist (MSA)
Cite as Authors (Year) Title. American Mineralogist, in press.
DOI: http://dx.doi.org/10.2138/am-2018-6049

Figure 6

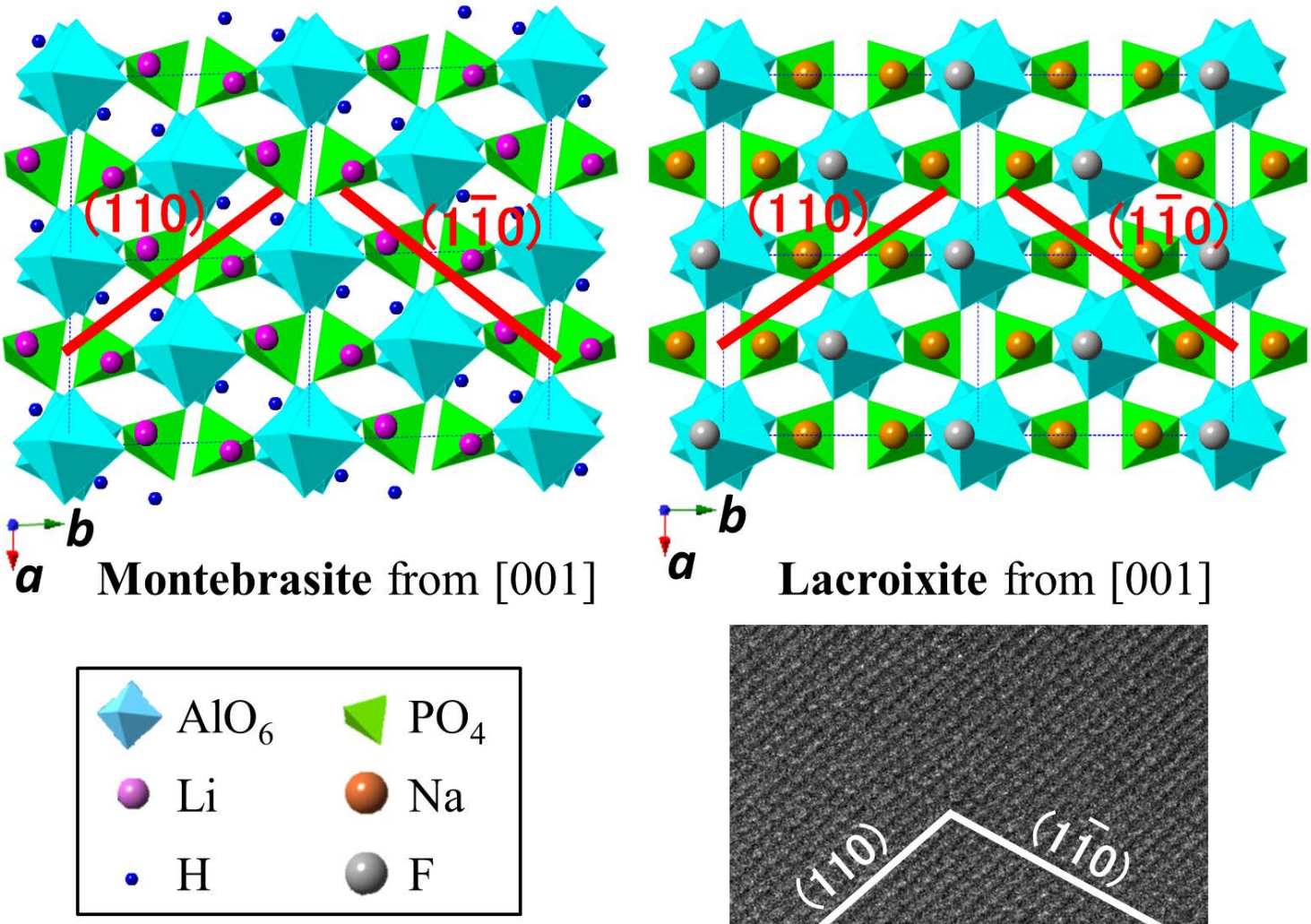

This is a preprint, the final version is subject to change, of the American Mineralogist (MSA)
Cite as Authors (Year) Title. American Mineralogist, in press.
DOI: http://dx.doi.org/10.2138/am-2018-6049

Figure 7

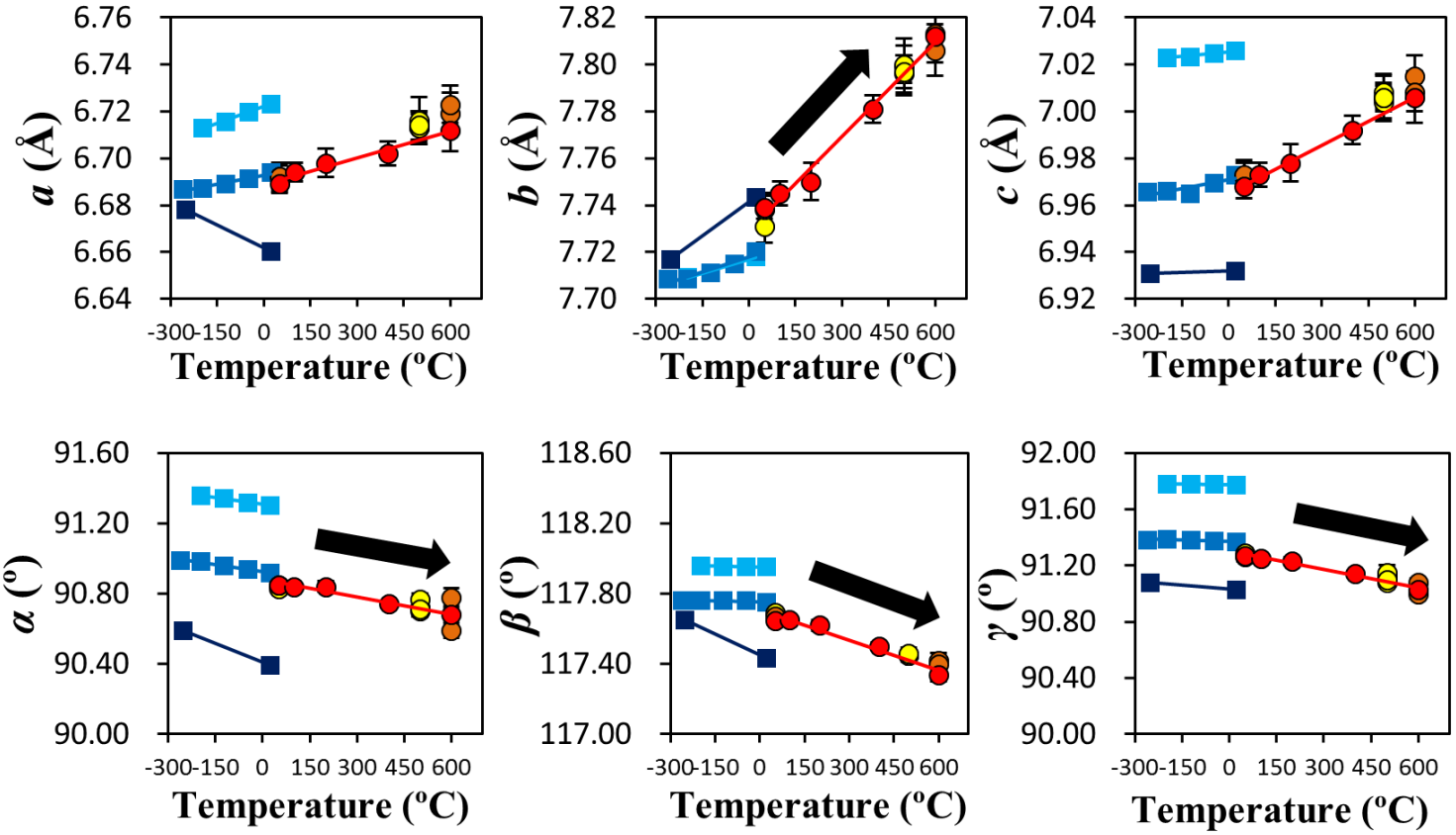

This is a preprint, the final version is subject to change, of the American Mineralogist (MSA)
Cite as Authors (Year) Title. American Mineralogist, in press.
DOI: http://dx.doi.org/10.2138/am-2018-6049

Figure 8

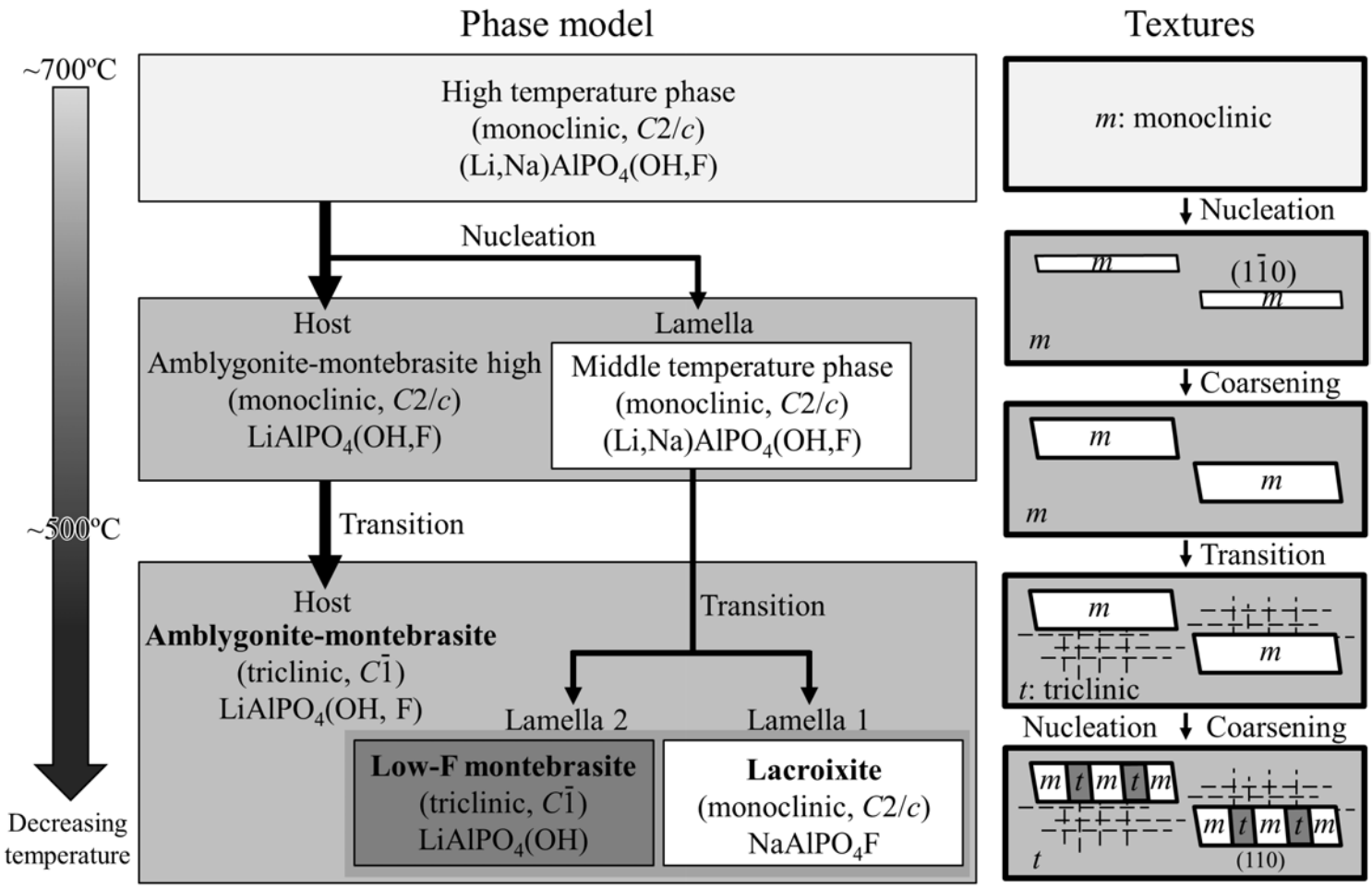

This is a preprint, the final version is subject to change, of the American Mineralogist (MSA)
Cite as Authors (Year) Title. American Mineralogist, in press.
DOI: http://dx.doi.org/10.2138/am-2018-6049

Figure 9

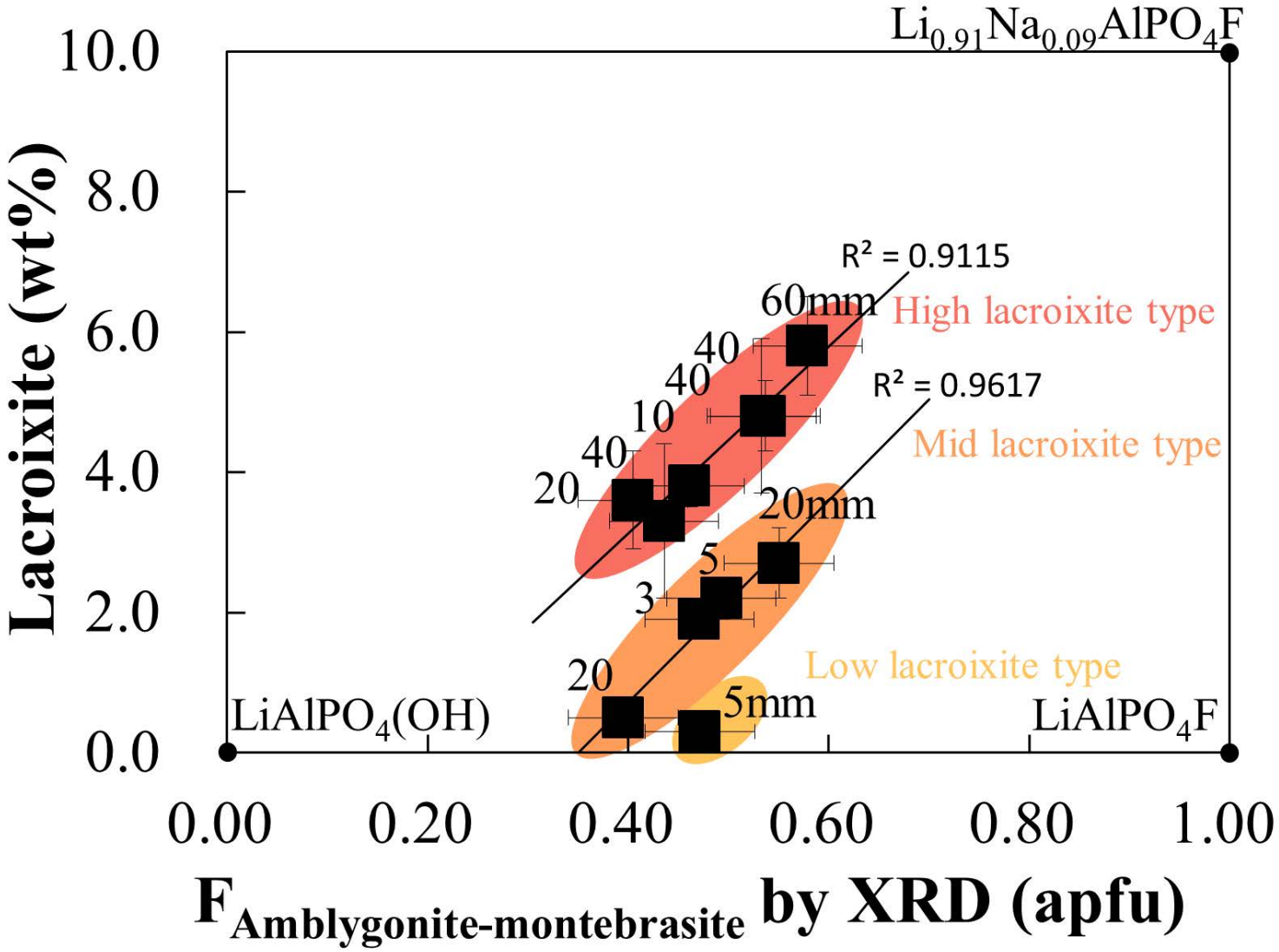

This is a preprint, the final version is subject to change, of the American Mineralogist (MSA)
Cite as Authors (Year) Title. American Mineralogist, in press.
DOI: http://dx.doi.org/10.2138/am-2018-6049

Figure 10

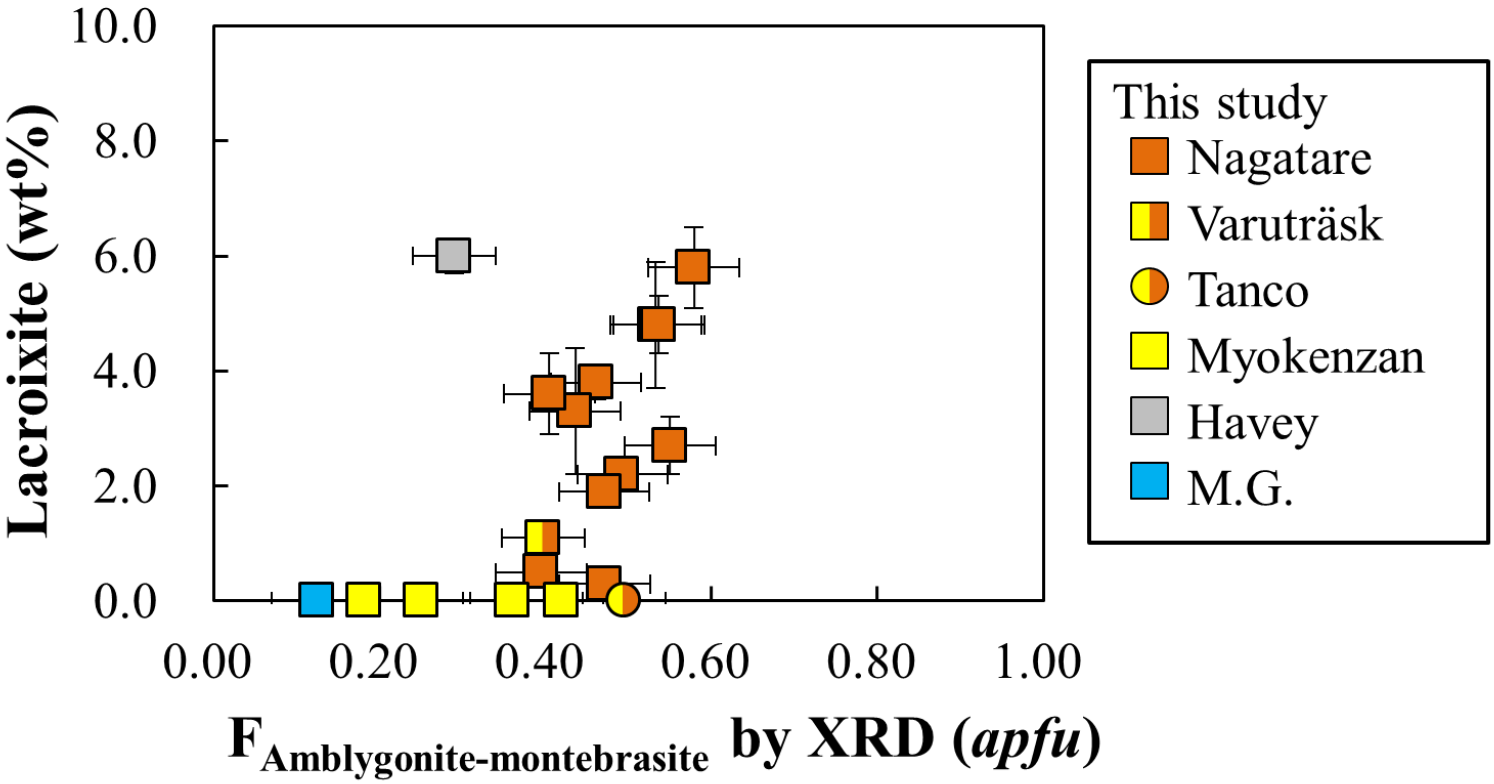

This is a preprint, the final version is subject to change, of the American Mineralogist (MSA)
Cite as Authors (Year) Title. American Mineralogist, in press.
DOI: http://dx.doi.org/10.2138/am-2018-6049

Figure 11